

Spectral properties of Shiba sub-gap states at finite temperatures

Rok Žitko^{1,2}

¹*Jožef Stefan Institute, Jamova 39, SI-1000 Ljubljana, Slovenia*

²*Faculty of Mathematics and Physics, University of Ljubljana, Jadranska 19, SI-1000 Ljubljana, Slovenia*

(Dated: January 20, 2016)

Using the numerical renormalization group (NRG), we analyze the temperature dependence of the spectral function of a magnetic impurity described by the single-impurity Anderson model coupled to superconducting contacts. With increasing temperature the spectral weight is gradually transferred from the δ -peak (Shiba/Yu-Shiba-Rusinov/Andreev bound state) to the continuous sub-gap background, but both spectral features coexist at any finite temperature, i.e., the δ -peak itself persists to temperatures of order Δ . The continuous background is due to inelastic exchange scattering of Bogoliubov quasiparticles off the impurity and it is thermally activated since it requires a finite thermal population of quasiparticles above the gap. In the singlet regime for strong hybridization (charge-fluctuation regime) we detect the presence of an additional sub-gap structure just below the gap edges with thermally activated behavior, but with an activation energy equal to the Shiba state excitation energy. These peaks can be tentatively interpreted as Shiba bound states arising from the scattering of quasiparticles off the thermally excited sub-gap doublet Shiba states, i.e., as high-order Shiba states.

PACS numbers: 72.15.Qm, 75.20.Hr

I. INTRODUCTION

A magnetic impurity in a superconducting host induces localized bound states inside the spectral gap, known in different communities as either Shiba, Yu-Shiba-Rusinov, or Andreev bound states^{1–9}. At zero temperature, Shiba states manifest as pairs of δ -peak resonances in the impurity spectral function $A(\omega)$ positioned symmetrically at positive and negative frequency corresponding to the transitions from the many-particle ground state to the *same* many-particle excited state by either adding a probing electron to the system ($\omega > 0$) or removing it ($\omega < 0$). The intrinsic temperature dependence of the spectral function depends on the impurity dynamics. When the impurity behaves as a classical object, i.e., a local magnetic field which is perfectly *static* on the time-scale of the experiment (“adiabatic limit” with no dynamics of the internal degrees of freedom of the impurity), the corresponding *classical* impurity model is a quadratic non-interacting Hamiltonian, hence the spectral function is not temperature dependent at all. This problem can be discussed in terms of single-particle levels and their occupancy. When the impurity behaves, however, as a quantum object, i.e., a *fluctuating* local moment as described by the Kondo or Anderson *quantum* impurity models, there will be non-trivial intrinsic temperature dependence due to electron-electron interactions (inelastic exchange scattering of thermally excited Bogoliubov quasiparticles off the impurity spin). This problem is better addressed from the perspective of many-particle eigenstates. Since the eigenvalue spectrum of the Hamiltonian operator includes both discrete Shiba states below the gap and a continuum part above the gap, it is expected that there will be both δ -peaks and a continuous background coexisting inside the gap at any finite temperature, providing a further realisation of the “bound state in the continuum” paradigm.

The temperature dependence of the Andreev spectra was studied experimentally in carbon nanotube quantum dots¹⁰. Strong temperature effects found in the measured differential conductance could be accounted for reasonably well us-

ing the tunneling formalism, however the intrinsic temperature dependence of the impurity spectral function was not discussed. Another experimental realization of impurity models are magnetic adatoms on superconducting surfaces. In Ref. 11 the measured differential conductance was discussed in terms of a phenomenological impurity model based on a classical impurity. There is, however, a lack of theoretical works on the temperature dependence of spectra of quantum impurity models to provide an alternative framework from the interpretation of measured spectra.

In this work we study the sub-gap spectral features in the single-impurity Anderson model with a superconducting bath described by the *s*-wave BCS mean-field Hamiltonian. After introducing the model and methods in Sec. II, we first consider the model by fixing the gap parameter Δ to its zero-temperature value and increasing the temperature T in Sec. III. This simplified calculation uncovers how the spectral weight is transferred from the Shiba δ -peak to the continuum. In this section we also study the hybridization dependence and the differences between the singlet (screened impurity) and doublet (unscreened impurity) regimes. In Sec. IV we perform a full calculation with the temperature dependent gap of a BCS superconductor; in this case the Shiba peak broadening is accompanied by peak shifts. We conclude with a discussion of the experimental relevance of the results.

II. MODEL AND METHOD

We consider the Hamiltonian $H = H_{\text{BCS}} + H_{\text{imp}} + H_{\text{c}}$:

$$\begin{aligned} H_{\text{BCS}} &= \sum_{k\sigma} \epsilon_k c_{k\sigma}^\dagger c_{k\sigma} - \Delta \sum_k \left(c_{k\uparrow}^\dagger c_{k\downarrow}^\dagger + \text{H.c.} \right), \\ H_{\text{imp}} &= \epsilon_d \sum_\sigma n_\sigma + U n_\uparrow n_\downarrow, \\ H_{\text{c}} &= \sum_{k\sigma} V_k \left(c_{k\sigma}^\dagger d_\sigma + \text{H.c.} \right). \end{aligned} \quad (1)$$

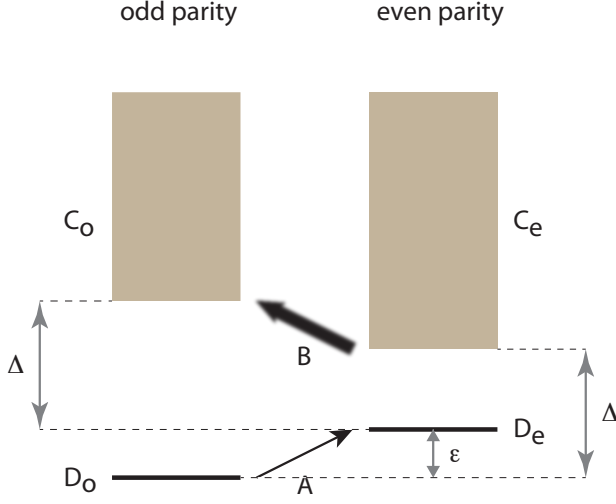


Figure 1. (Color online) Schematic diagram of the many-particle eigenstates of the Hamiltonian, partitioned into the even and odd fermion-parity sectors (i.e., parity of the total electron number). This diagram corresponds to the case where the ground state has odd parity (spin-doublet). D_o and D_e are the odd-parity (spin-doublet) $|D\rangle$ and the even-parity (spin-singlet) $|S\rangle$ discrete eigenstates. The even-parity continuum C_e starts at energy Δ above the odd-parity discrete state D_o , since the bottom-most states of the continuum are composed of one additional quasiparticle added to D_o , thus changing the overall fermion parity. The odd-parity continuum C_o starts at energy Δ above the even-parity discrete state D_e , for similar reasons. Note that the multiple-quasiparticle states have energies at least 2Δ above D_o . Label A indicates a sharp transition (contributing a δ -peak to the impurity spectrum), label B diffuse transitions (contributing a continuous background to the spectrum).

Here $c_{k\sigma}$ and d_σ are the band and impurity electron annihilation operators, ϵ_k the band dispersion relation, Δ the BCS gap parameter, ϵ_d the impurity level, U the electron-electron repulsion, $n_\sigma = d_\sigma^\dagger d_\sigma$ the impurity occupancy operator, and V_k the hopping integrals. The Hamiltonian does not include any coupling to electromagnetic noise or phonons.

Assuming a flat band with the density of states ρ in the normal state, and $V_k \equiv V$, the impurity coupling is fully characterized by the hybridization strength $\Gamma = \pi\rho V^2$. In this work, we focus on the particle-hole (p-h) symmetric case with $\epsilon_d = -U/2$. The Kondo exchange coupling at $\Delta = 0$ is given by the Schrieffer-Wolff transformation as $\rho J_K = 8\Gamma/\pi U$ and the Kondo temperature as¹²

$$T_K^0 \sim U\sqrt{\rho J_K} \exp\left(-\frac{1}{\rho J_K}\right). \quad (2)$$

In the superconducting case with $\Delta \neq 0$, the ground state of the system is either a singlet $|S\rangle$ or a doublet $|D\rangle$ depending on the value of the ratio Δ/T_K^0 . All other eigenstates are, in the first approximation (i.e., neglecting residual interactions between the quasiparticles), product states of either $|S\rangle$ or $|D\rangle$ with additional Bogoliubov quasiparticles from the continuum. While the total particle number is not a conserved quantum number for $\Delta \neq 0$, its parity is. The eigenstates can

thus be classified into odd and even fermion parity sectors, as illustrated for the case of an odd-parity (spin doublet) ground state in Fig. 1. A quasiparticle is an object with odd fermion-parity, thus the even-parity continuum starts at the energy Δ above the odd-parity ground state, while the odd-parity continuum starts at the energy $\epsilon + \Delta$ above the ground state, where ϵ is the Shiba state “energy” (more precisely, the energy difference

$$\epsilon = |E_S - E_D| \quad (3)$$

between the sub-gap many-particle Shiba states).

In this work we are interested mainly in the spectral functions at finite T . The calculations are performed with the numerical renormalization group (NRG)^{3,13–20}. This method appears at first perfectly suited for the problem, since it is an unbiased nonperturbative numerical technique, applicable both at zero and at finite temperatures, which can handle arbitrary bath density of states (including with a superconducting gap), and provides the spectral function directly on the real frequency axis. Other methods are either biased, perturbative, inapplicable to the superconducting case, or require an analytical continuation from the Matsubara axis to real frequencies; in particular, this last issue makes the quantum Monte Carlo (QMC) approach of little use, since it is extremely difficult to perform an analytical continuation in the presence of a sharp gap, especially since it is necessary (see below) to resolve a δ -peak superposed on a continuous background of finite support inside the gap. Nevertheless, the situation under study in this work is in some regards perhaps the worst possible case for the NRG. While the method works very well for problems with spectral gap at zero temperature, and for non-gapped baths at any temperature, there are severe difficulties when both Δ and T are non-zero. Both the gap and the temperature break the scale invariance on which the method is based, and they do so in different ways, thereby generating inevitable systematic errors. The results for spectral functions presented in this work should thus be considered as qualitatively correct, while quantitative errors are estimated (by monitoring how the results fluctuate when the NRG calculation parameters are varied) to be in the tens of percent range for $T \sim \Delta$. In spite of this shortcoming, there is presently no other impurity solver to meaningfully study the finite-temperature spectral function. Static properties, such as the expectation values of various operators, can be reliably computed using the QMC^{21,22}. Even here, there are some small systematic discrepancies between the QMC and NRG when both Δ and T are non-zero. Such comparisons of static properties are very useful to tune the parameters of the NRG to values where such discrepancies are minimal. Finally, we note that the finite-temperature problems in the NRG become severe when U is small, while they seem to be more manageable in the deep Kondo regime which is of main interest in this study.

The NRG calculations were performed with the discretization parameter $\Lambda = 2$, with $N_z = 8$ interleaved discretization grids^{23,24}, using the full-density-matrix algorithm with the Wilson chain terminated at the energy scale $E_{\text{chain}} = \Delta/50$ ^{25–27}. The “traditional” choice of the discretization parameter $\Lambda = 2$ proved to be near optimal. The results depend

little on the choice of the discretization method²⁴. The length of the Wilson chain, however, turned out to be a critical parameter and had to be tuned.

To obtain a good description of the continuum part of the sub-gap spectrum at finite temperatures, it furthermore proved crucial to keep a large number of states in the NRG iteration even at energy scales below Δ , much more than required for obtaining well converged thermodynamics and $T = 0$ spectral functions; we kept at least 2500 multiplets. While computationally demanding, this is critically important for a good description of the continuum quasiparticle spectrum in both even- and odd-parity parts of the full Fock space.²⁸

The impurity Green's function is defined as

$$G(t) = -i\theta(t)\text{Tr} \{ \rho[d_\sigma(t), d_\sigma^\dagger(0)]_+ \}, \quad (4)$$

where the trace is evaluated with the grand-canonical density matrix $\rho = e^{-\beta H}$ (the chemical potential is fixed to $\mu = 0$). This is an appropriate description only for well equilibrated ergodic systems. The assumption of ergodicity is non-trivial and may not be valid in all impurity systems and under all experimental conditions. Furthermore, the presence of the tunneling contacts will drive the system out of equilibrium.

The impurity spectral function,

$$A(\omega) = -\frac{1}{\pi} \text{Im} \tilde{G}(\omega + i\delta), \quad (5)$$

where \tilde{G} is the Fourier transform of G , can be expressed using the Lehmann decomposition as

$$A(\omega) = \frac{1}{Z} \sum_{mn} |\langle m|d_\sigma|n \rangle|^2 \times (e^{-\beta E_m} + e^{-\beta E_n}) \delta(\omega + E_m - E_n), \quad (6)$$

where m, n index all eigenstates of the Hamiltonian, $E_{m,n}$ are the corresponding eigenvalues, $\beta = 1/k_B T$, and the grand-canonical partition function is $Z = \text{Tr}[\exp(-\beta H)] = \sum_m \exp(-\beta E_m)$. The actual calculation of $A(\omega)$ is performed using the full-density-matrix algorithm²⁷, generalizing the complete-Fock-space approach^{25,26}. We accumulate the raw spectral data separately for $|\omega| < \Delta$ and $|\omega| > \Delta$. Inside the gap, we use 5000 equidistant bins. Outside the gap, we use a logarithmic mesh of bins with low-frequency accumulation points at $\omega = \pm\Delta$ and with 1000 bins per frequency decade. This modification of the standard binning is necessary for obtaining constant spectral resolution inside the gap and a correct description of the gap edges in the continuum above the gap²⁹.

The Green's function probes the single-particle excitations of the system. It should be emphasized that all contributions to G correspond to electron-parity-changing transitions (see Fig. 1). Let us consider the doublet regime, where the impurity spin is unscreened and the ground state is the odd-parity spin-doublet $|D\rangle$. At zero temperature, only the ground state D_o is thermally occupied, and the only transition with $\Delta E < \Delta$ is that to the discrete excited state D_e (transition A indicated by the sharp arrow in Fig. 1). The sub-gap part

of the spectrum is thus fully described by two δ -peaks at positions $\omega = \pm\epsilon$ with equal weight (due to the p-h symmetry) given by

$$w_\delta(T=0) = \frac{1}{2} |\langle D_o|d_\sigma|D_e \rangle|^2. \quad (7)$$

At finite temperatures there are further transitions with starting and end states separated by less than Δ : they are indicated by a diffuse arrow B in Fig. 1 and correspond to transitions from the thermally populated even-parity quasiparticle states at energies above Δ (set C_e) to the odd-parity quasiparticle states at energies above $\epsilon + \Delta$ (set C_o). Since the states involved form continua, this will generate a continuous spectral weight contribution to the sub-gap spectrum. The most likely transitions are those from the bottom of C_e to the bottom of C_o , thus the continuum background is expected to be peaked at $|\omega| = \epsilon$, i.e., at the position of the discrete Shiba state which itself persists at finite temperature at least up to $T \sim \Delta$. The evolution with increasing T is thus expected to be as follows: the weight of the δ -peak decreases, while the weight of a new broad peak centered at the same position increases. In the limit of high temperatures, $T \gg \Delta$, the partition function Z is large, the discrete contribution A to the spectral function is negligible and there is only continuum weight (this happens in the $T \rightarrow T_c$ limit, where $\Delta(T) \rightarrow 0$). In the next sections, we confirm this intuitive physical picture by numerical calculations.

III. RESULTS: FIXED Δ

A. Overview and main characteristics

The calculations in this subsection are performed for fixed model parameters ($\Gamma/U = 0.1$ and $U/\Delta = 20$), only the temperature T is variable. The ground state is a spin doublet, while the singlet excited state lies at the energy level

$$\epsilon = 0.423\Delta \quad (8)$$

above it. Due to the p-h symmetry the spectral function is even and we focus on its $\omega > 0$ (particle addition) part. At zero temperature, the weight of the δ -peak at $\omega = \epsilon$ is

$$w_\delta(T=0) = 0.0341. \quad (9)$$

This indicates that the Shiba bound state wavefunction (as far as it can be defined for an interacting system) has majority of its weight not on the impurity, but in the host, which is commonly the case for Shiba states.

At finite temperatures some care is required in post-processing the raw spectral data as obtained from the NRG run. The δ -peak is extracted from the spectral function by removing the weight in a narrow interval of width $2 \times 10^{-4}\Delta$ around $\omega = \epsilon$, where ϵ can be independently determined very accurately from the NRG flow diagrams. The remaining continuous part of the spectral function is then broadened and further characterized. This procedure allows us to reliably parti-

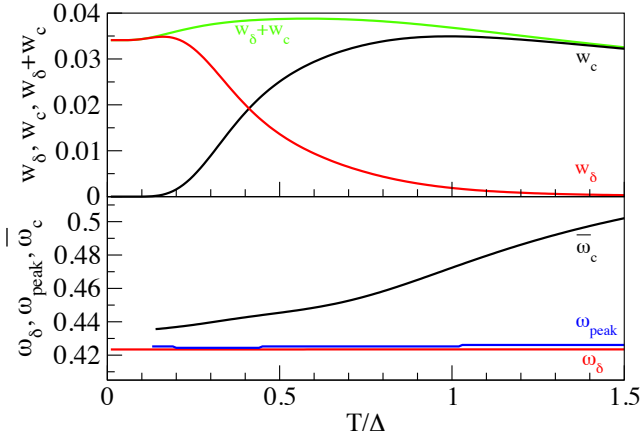


Figure 2. (Color online) (a) δ -peak, continuum, and total spectral weight in the positive-frequency sub-gap part ($0 < \omega < \Delta$) of the impurity spectral function $A(\omega, T)$. (b) Position of the δ -peak, ω_δ , and of the maximum of the continuous part, ω_{peak} , as well as the mean value of the continuous part, $\bar{\omega}_c$.

tion the spectral function into discrete and continuous components:

$$A(\omega) = A_\delta(\omega) + A_c(\omega). \quad (10)$$

The corresponding spectral weights are defined as

$$w_i = \int_0^\Delta A_i(\omega) d\omega \quad (11)$$

with $i = \delta, c$. It should be noted in passing that at finite temperatures $w_\delta(T)$ receives contributions not only from the transition A, but also from a discrete subset of transitions between the states forming the continua C_e and C_o with energy difference *exactly* equal to ϵ (i.e., the transitions $D_e \rightarrow D_o$ in the presence of quasiparticles, but without the quasiparticles interacting with the impurity). The temperature dependence of both w_δ and w_c is an interaction effect: for a non-interacting Hamiltonian, such as that corresponding to a classical impurity with no internal dynamics, the spectral function itself would not depend in any way on the temperature (although the *occupancies* of the single-particle levels would change with T).

The most important spectral characteristics are revealed in the temperature-dependence plots shown in Fig. 2, while an example of a typical finite- T spectral function is shown in Fig. 3.

The continuum weight w_c exhibits activated behavior for low T , with the activation energy Δ :

$$w_c(T) = 0.168 e^{-\Delta/T}. \quad (12)$$

This confirms the expectation that the continuum background is associated with the *inelastic* transitions that require a finite thermal population of the quasiparticle states above the gap which scatter on the impurity (diffuse transitions as shown schematically in Fig. 1, arrow B).

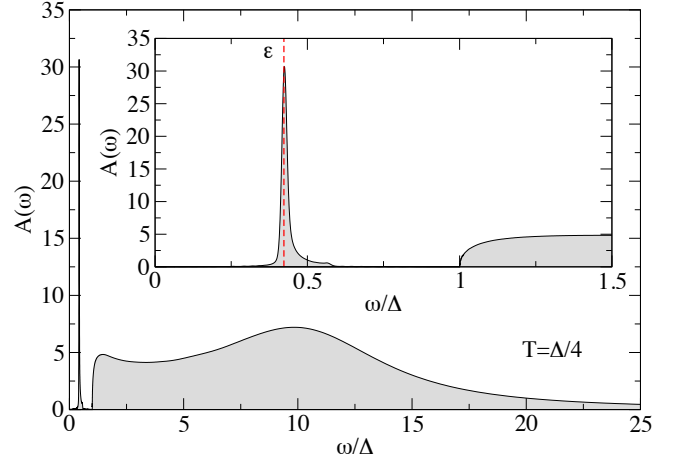


Figure 3. (Color online) Impurity spectral function $A(\omega, T)$ at finite temperature $T = \Delta/4$. The hump at $\omega = 10\Delta = U/2$ is the Hubbard peak. The inset shows a close-up on the sub-gap region. The position of the δ -peak, ϵ , is indicated using the dashed line and essentially coincides with the peak of the continuum part.

For $T \gtrsim 0.2\Delta$, w_δ is a strictly decreasing function of temperature, while w_c is increasing, and their sum $w_\delta + w_c$ is approximately constant: the weight is gradually transferred from the coherent discrete Shiba state to diffuse states involving itinerant quasiparticle states, i.e., this represents a thermal decomposition of the Shiba state. We note that $w_\delta = w_c$ on the scale $T \approx \Delta/2$. This is also the range where the total weight $w_\delta + w_c$ reaches a maximum value. The continuum weight w_c is increasing up to $T \approx \Delta$ where it reaches a value close to $w_\delta(T = 0)$. In simple terms, with increasing temperature almost all spectral weight is transferred from the δ -peak to the continuum by $T \approx \Delta$. For $T > \Delta$, w_c itself becomes a decreasing function, albeit only weakly: the decay of w_δ at large T is much faster than that of w_c , and w_δ becomes essentially zero by $T \approx 2\Delta$.

In Fig. 2(b) we consider the peak positions. The δ -peak does not move with temperature. This is expected, since its position $\omega_\delta = \epsilon$ is given by the energy difference of the two discrete eigenstates of the Hamiltonian, thus it is a property of the operator itself and has nothing to do with thermal effects. The continuum part of the sub-gap spectrum is a peaked function, see Fig. 3. The position of this peak, ω_{peak} , almost coincides with the δ -peak position:

$$\omega_{\text{peak}} \approx \omega_\delta = \epsilon. \quad (13)$$

ω_{peak} is very weakly temperature dependent, see Fig. 2(b). We also plot the mean of the continuum part, $\bar{\omega}_c$, defined as the normalized first moment of $A_c(\omega)$. The mean is larger than ϵ and further increases with T , indicating that the continuum part of the spectrum is skewed toward larger frequencies, as can also be seen in Fig. 3. At low temperatures, the skewness exceeds 6. The long tail is due to the asymmetry of the transitions: the most populated thermally excited starting states are those near the bottom of the even-parity continuum and most likely end states those at the bottom of the odd-parity

continuum starting at ϵ higher in energies. At higher temperatures, $T \sim \Delta$, the distribution becomes more symmetric around $\omega = \epsilon$ with a clear dominant peak, corresponding to the “thermally broadened” Shiba resonance.

The width of the continuum part can be further characterized through the standard deviation (not shown). It is a strictly increasing function of T . At intermediate temperatures $T \approx \Delta/2$ it reaches a value of order 0.1Δ , thus the background is relatively broad. Another relevant quantity is the half-width at half-maximum (HWHM) of the main peak in the continuum part. This quantity is very difficult to extract reliably since it requires a delicate broadening procedure and it strongly depends on the NRG calculation parameters. We find that the HWHM is only weakly increasing in the temperature range $T < \Delta$: it starts at values close to 0.01Δ in the low-temperature limit and increases to $\sim 0.015\Delta$ at $T = \Delta$. The main thermal effect is thus the weight transfer from the discrete to the continuous part, but there appears to be little broadening in the sense of decreasing lifetime of the continuum resonance feature at $\omega = \epsilon$.

B. Γ -dependence

We now study how the results from the previous subsection depend on the value of the hybridization Γ , in particular across the singlet-doublet quantum phase transition where $|S\rangle$ and $|D\rangle$ interchange their roles as the ground and the excited state, respectively.

For low enough Γ , so that the impurity is in the Kondo regime, the Shiba state energy ϵ follows the universal dependence $\epsilon(T_K/\Delta)$, where $T_K = T_K(\Gamma)$. For $\Gamma \rightarrow 0$, the peak is close to the gap edge, then it moves toward the chemical potential for increasing Γ , see Fig. 4. For chosen $U/\Delta = 20$, the singlet-doublet (S-D) transition occurs at

$$\Gamma_c = 0.155U. \quad (14)$$

We first consider how the temperature dependencies of the key spectral characteristics change for different values of Γ . The δ -peak position $\omega_\delta = \epsilon$ does not vary with temperature. The continuum mean, ω_c , shown in Fig. 5, starts from $\omega_c(T=0) \approx \epsilon$ for $\Gamma < \Gamma_c$, while for $\Gamma \gtrsim \Gamma_c$ it starts from values close to the gap edge (this peculiar low-temperature behavior will be explained in subsection III C). In the temperature range $T \lesssim \Delta$, ω_c is a decreasing function of T for all cases where ϵ is close to the gap edge (i.e., in deep doublet and in deep singlet phases), while it is non-monotonic or increasing for $\epsilon \ll \Delta$ (i.e., in the transition range with Shiba states deep in the gap), see Fig. 5.

The continuous-background weight w_c is strictly increasing as a function of Γ at any fixed T up to

$$\Gamma^* \approx 0.225U, \quad (15)$$

see Fig. 6. For $\Gamma \lesssim \Gamma^*$, the system is in the regime of well defined local-moment (the Hartree-Fock solution spin polarizes for $\Gamma < U/\pi \approx 0.3U$) with properties controlled by the ratio Δ/T_K , while for $\Gamma \gtrsim \Gamma^*$ the charge fluctuations are important

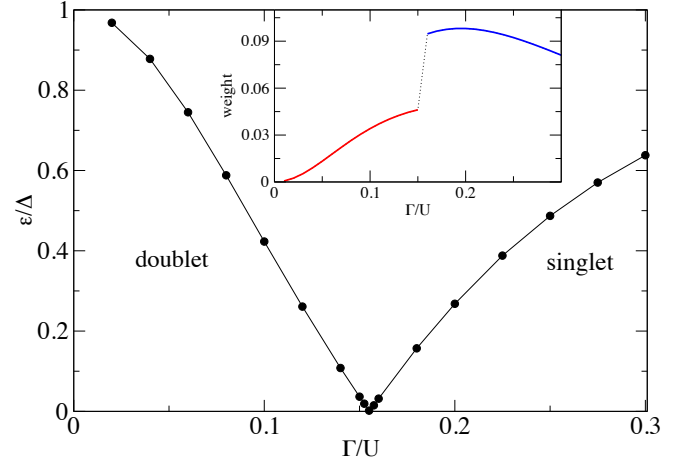


Figure 4. (Color online) Shiba state energy ϵ as a function of the hybridization strength Γ , for fixed $U/\Delta = 20$. The inset shows the $T = 0$ spectral weight of the sub-gap δ -peak.

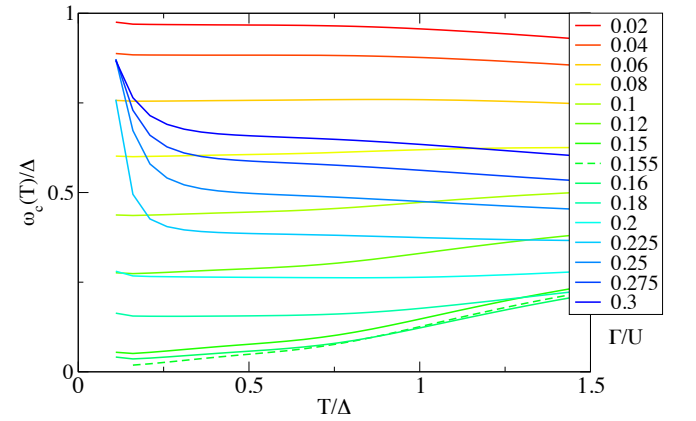


Figure 5. (Color online) Temperature dependence of the mean-value of the continuum part of the sub-gap spectrum, $\omega_c(T)$, for a range of hybridization strengths Γ .

and the impurity properties become non-universal. At low T , the same exponential law $w_c = b e^{-\Delta/T}$ is found for all values of $\Gamma \lesssim \Gamma^*$, both in the singlet and in the doublet regimes, with $b(\Gamma)$ dependence which can be read off from Fig. 6(b). For $\Gamma \gtrsim \Gamma^*$, however, we find some deviations from pure exponential dependence. The maximum in $w_c(T)$ is always on the scale $T \sim \Delta$.

The δ -peak weight is monotonically decreasing as a function of T for small Γ and has a local maximum for intermediate $\Gamma < \Gamma_c$, see Fig. 7. The temperature of the maximum shifts to lower temperatures as Γ increases toward Γ_c and for $\Gamma > \Gamma_c$ the weight again becomes a monotonically decreasing function of T . This pronounced difference in the low- T regime for $\Gamma \approx \Gamma_c$ can serve as a tool to distinguish between the doublet and singlet regimes at finite temperatures. Indeed, in the zero-temperature limit and in the absence of magnetic field (as assumed throughout this work) the sub-gap weight changes discontinuously by a factor of 2 across the S-D transition, see the inset to Fig. 4. At finite T , this discontinuity

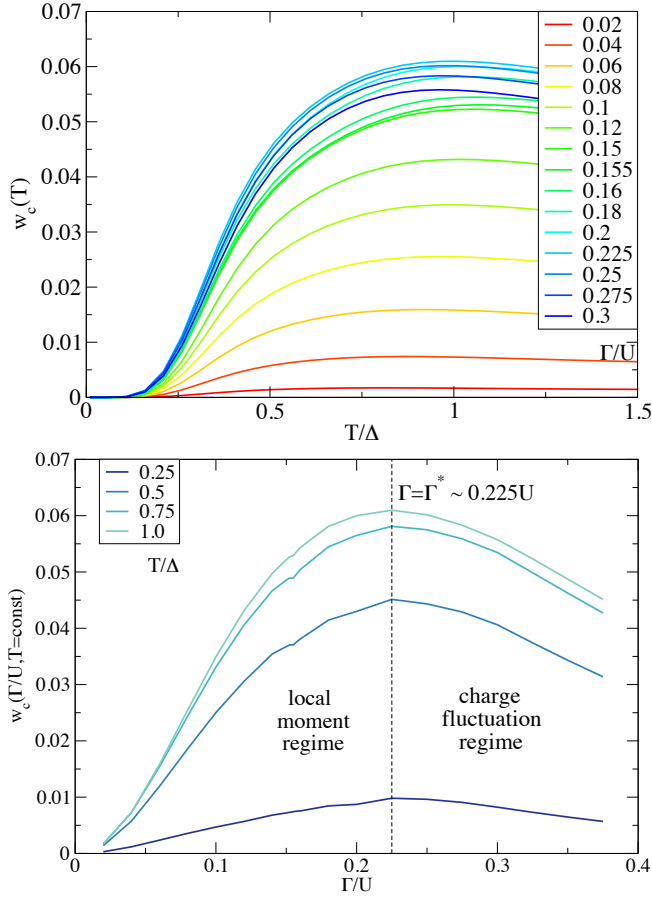


Figure 6. (Color online) (a) Temperature dependence of the continuum part weight, $w_c(T)$, for a range of hybridization strengths Γ . (b) Γ -dependence for a range of fixed temperatures.

is washed out, see the inset to Fig. 7. The up/down-turn of $w_\delta(T)$ occurs at $T \approx |\epsilon|$, and this scale moves toward 0 as $\Gamma \rightarrow \Gamma_c$, as shown in the main panel of Fig. 4.

For $\Gamma > \Gamma^*$ the charge fluctuations lead to a decreasing sub-gap spectral weight. The decreasing trend is also related to the fact that the δ -peak moves close to the gap edge in the limit $\Gamma \gg \Gamma^*$. This is a known effect: Shiba states merge with the continuum in a continuous way by transferring spectral weight from the δ -peak to the quasiparticle part, so that the weight of the δ -peak goes to zero as its position approaches $\omega = \Delta$.

C. High-order Shiba states for large Γ

Several anomalies are observed for large values of Γ . Their common origin is an additional sub-gap spectral peak just below the gap edge, see Fig. 8. The weight of this peak shows activated behavior at low temperatures:

$$w_2(T) = 0.018e^{-\epsilon/T}, \quad (16)$$

where $\epsilon = 0.637\Delta$ for the chosen value $\Gamma/U = 0.3$. This peak dominates the continuum background for small T , because its activation energy ϵ is lower than that (Δ) of the

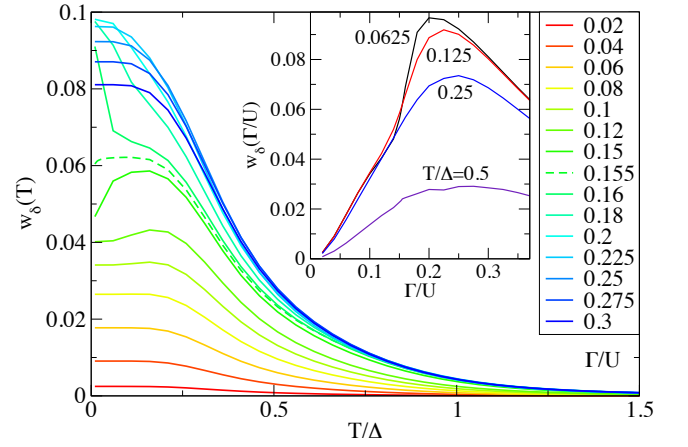


Figure 7. (Color online) Temperature dependence of the δ -peak weight, $w_\delta(T)$, for a range of hybridization strengths Γ .

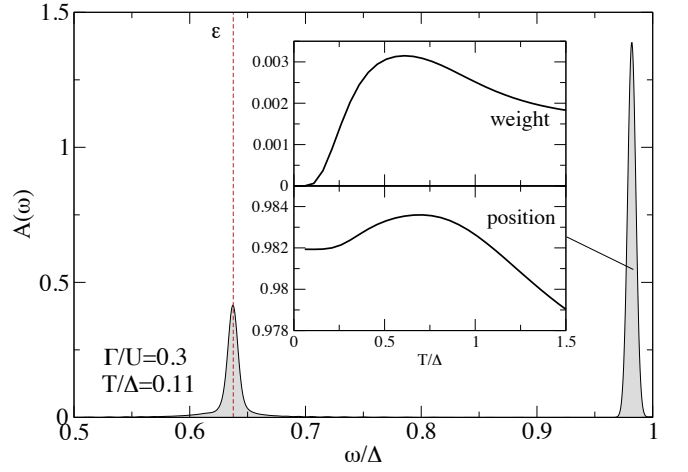


Figure 8. (Color online) Sub-gap spectrum for strong hybridization $\Gamma = 0.3U$. The inset shows the temperature dependence of the weight and position of the secondary ‘‘high-order Shiba’’ peak which appears just below the gap edge.

continuous background centered around the Shiba peak. The dominance of the extra peak in the $T \rightarrow 0$ limit explains the strikingly peculiar low- T behavior of $w_c(T)$ in Fig. 5. Extensive testing has been performed to assess if this feature could merely be a numerical artifact of the NRG method. Varying Λ , Wilson chain length, the discretization scheme, the algorithm for computing the spectral function (naive Lehmann-decomposition approach, complete-Fock-space, full-density-matrix), and the number of states kept in the truncation, it was found that this feature persists. It is thus either a generic artifact of the method for finite T and Δ that cannot be eliminated by any parameter choice, or a real spectral feature of the Anderson impurity model with superconducting baths. Presently, there is no other theoretical method to reliably confirm the presence of this peak. However, the spectral weight appears sufficiently large that it could be detected experimentally, despite its vicinity to the gap edge.

It should be emphasized that there are no discrete sub-

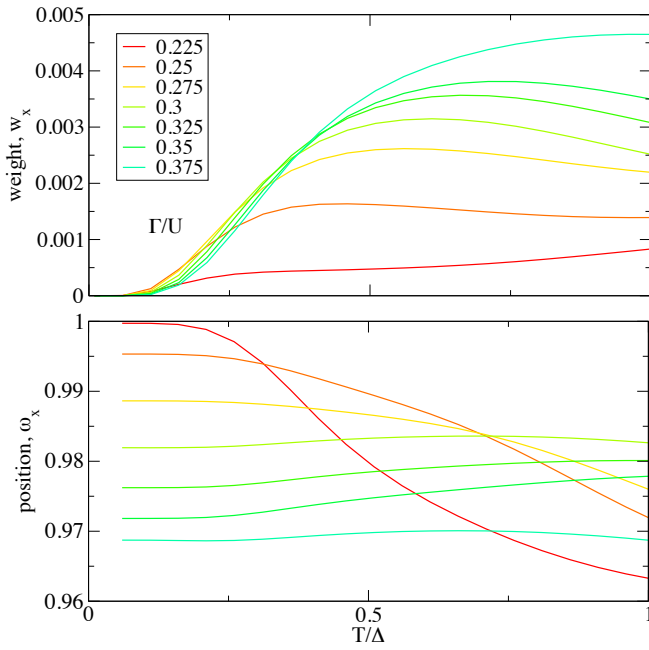


Figure 9. (Color online) Weight and position of the “high-order Shiba peak” below the gap edge.

gap multi-particle states with the energy corresponding to this peak. Instead, its origin is associated with quasiparticle scattering on the *thermally* excited doublet Shiba state $|D\rangle$ (for large Γ , the ground state is namely $|S'\rangle$), generating new bound states of Bogoliubov quasiparticles. In fact, it can be argued that the physical mechanism is essentially the same as for the conventional Shiba states: by thermal occupation of the doublet excited states at finite temperatures the impurity partially “remagnetizes”, and its magnetic moment couples to the superconducting bath via an effective exchange coupling constant proportional to $J_K w_D$, where $J_K \propto \Gamma/U$ and $w_D = e^{-\epsilon/T}/Z(T)$ is the average population in the doublet state. This generates a bound state located just below the gap edge because the effective coupling is weak. This picture is certainly oversimplified and fails to explain, for example, the relatively constant position of the peak as a function of temperature. Nevertheless, it is interesting that such “high-order Shiba states” can be generated at finite temperatures.

Fig. 9 shows the Γ -dependence of the weight and position of the additional peak. The threshold for the existence of the peak is related to Γ^* , thus the peak is intimately related to entering the charge-fluctuation regime. Close to the threshold, its $T = 0$ position is at the gap-edge, while for larger Γ it starts at a finite binding energy below the edge.

IV. RESULTS: BCS $\Delta(T)$

We now consider a realistic case where the gap Δ is temperature dependent and tends to zero as the critical temperature T_c is approached. We use a simplified phenomenological

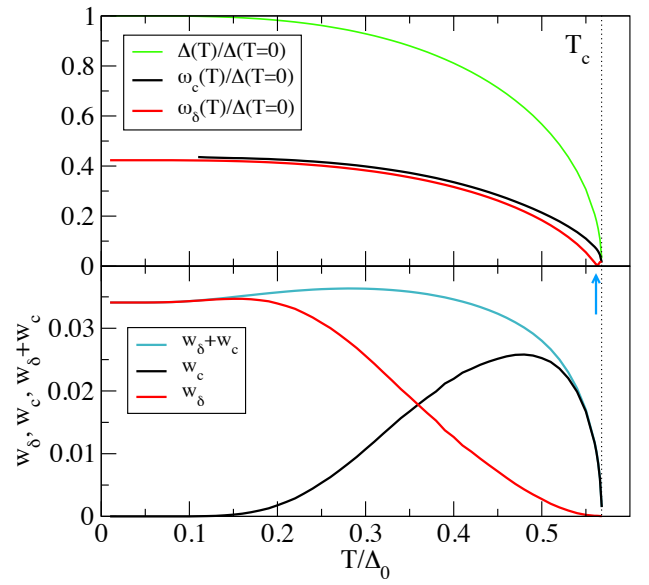


Figure 10. (Color online) Temperature dependence of the quantities characterizing the sub-gap spectral function in the case of $\Delta = \Delta_{\text{BCS}}(T)$. The temperature driven doublet-singlet phase transition is indicated by the arrow. Model parameters are $\Gamma/U = 0.1$ and $U/\Delta = 20$.

expression

$$\Delta_{\text{BCS}}(T) \approx \delta_{sc} T_c \tanh \left[\frac{\pi}{\delta_{sc}} \sqrt{a \frac{\delta C}{C_N} \left(\frac{T_c}{T} - 1 \right)} \right] \quad (17)$$

with $\delta_{sc} = 1.76$, $a = 2/3$, $\delta C/C_N = 1.43$, which is a good approximation for the true BCS temperature dependence with correct $T \rightarrow 0$ and $T \rightarrow T_c$ asymptotics.

We consider the case where the system is in the doublet regime at $T = 0$. The temperature dependence of key quantities is shown in Fig. 10. The reduction of Δ with increasing T drives the system toward the singlet regime. The doublet-singlet transition occurs, however, just before the critical point (indicated by the arrow in the figure). Although occurring at a finite temperature, such first-order boundary transition corresponds to a change of the ground state of the impurity+bath system by the variation of an “external” parameter, thus it may still be considered as a quantum phase transition of the impurity subsystem (formed by the impurity itself and the subset of host states which hybridize with the impurity), even though it is actually driven by thermal fluctuations in the superconducting host which drive down the gap function $\Delta(T)$.

V. DISCUSSION

Based on general considerations of an interacting impurity system, and confirmed by numerical calculations, Shiba states at finite temperature lose spectral weight to a continuous sub-gap background centered at the same position. This immediately leads to a question of principle about the proper definition of the intrinsic lifetime of a Shiba state. A discrete

excited many-particle state isolated from the continuum could be expected to not decay at all. This is clearly the case in the absence of quasiparticles. In an open system at finite temperature, i.e., in contact with a heat and particle reservoir, a quasiparticle in the superconductor can be generated through a thermal fluctuation and can interact with the impurity spin, giving rise to a continuum background. The excited Shiba state can release its excitation energy to the quasiparticle and decay to the Shiba ground state, resulting in a finite lifetime.

The model system studied here is admittedly simplistic. In relativistic systems, in particular when there are tunneling pathways to a normal metal (such as a normal-state tip of a scanning tunneling microscope), the δ -peak will strictly speaking no longer exist. Similarly, (direct or indirect) coupling to the acoustic phonons of the host will broaden the δ -peak. If such couplings are small, however, it may still be expected that the impurity spectral function will be multimodal with non-trivial temperature dependence.

Let us now consider the example of Mn adatoms on Pb(111) studied in Ref. 11. Pb has $T_c = 7.2$ K or $\Delta_0 \approx 1.1$ meV. The experimental temperatures were 1.2 K and 4.8 K. Taking into account the reduction of Δ in the BCS theory, these correspond to $k_B T / \Delta$ of 0.12 and 0.41, respectively. The lower temperature is thus in the low- T limit, while at the second one the finite-temperature effects are expected to be sizable. In experiments, at the lower temperature the measured linewidth was resolution limited and had to be estimated indirectly through current saturation plateaus. At the higher temperature, the width could be extracted from the peak width in the weak-coupling regime, giving $\Gamma \approx 0.2$ meV. Thus

$\Gamma / \Delta_0 \approx 0.2$. Even without discussing how to properly quantify the intrinsic lifetime in NRG calculations (lower bound is the HWHM of the continuum peak, $\sim 0.01\Delta$, upper bound is the standard deviation of the continuum, $\sim 0.1\Delta$), it is possible to conclude that the order of magnitude is roughly correct. It should be noted that there are further relaxation mechanisms (such as fermion-parity-conserving transitions assisted by phonons and photons) not included in our model, which are likely to be comparable to the “intrinsic” broadening due to electron-electron interactions, but the intrinsic mechanism is certainly not negligible.

This work opens up a number of interesting issues for further study. One could study how the intrinsic temperature dependence of the spectral function is reflected in the transport properties. This is relevant for scanning tunneling spectroscopy studies of single impurities and adatom chains, such as those expected to host Majorana end modes. Another question is how the results are modified if the BCS mean-field Hamiltonian is replaced by a proper interacting model with electron-electron attraction terms. Finally, we need better theoretical understanding of the “high-order Shiba states” and their relation to the charge fluctuations.

ACKNOWLEDGMENTS

I acknowledge discussions with Tomaž Rejec and Jernej Mravlje, and the support of the Slovenian Research Agency (ARRS) under Program No. P1-0044.

-
- ¹ H. Shiba, “Classical spins in superconductors,” *Prog. Theor. Phys.* **40**, 435 (1968).
 - ² H. Shiba, “A Hartree-Fock theory of transition-metal impurities in a superconductor,” *Prog. Theor. Phys.* **50**, 50 (1973).
 - ³ Koji Satori, Hiroyuki Shiba, Osamu Sakai, and Yukihiro Shimizu, “Numerical renormalization group study of magnetic impurities in superconductors,” *J. Phys. Soc. Japan* **61**, 3239 (1992).
 - ⁴ A. V. Balatsky, I. Vekhter, and Jian-Xin Zhu, “Impurity-induced states in conventional and unconventional superconductors,” *Rev. Mod. Phys.* **78**, 373 (2006).
 - ⁵ A. Yazdani, B. A. Jones, C. P. Lutz, M. F. Crommie, and D. M. Eigler, “Probing the local effects of magnetic impurities on superconductivity,” *Science* **275**, 1767 (1997).
 - ⁶ R. S. Deacon, Y. Tanaka, A. Oiwa, R. Sakano, K. Yoshida, K. Shibata, K. Hirakawa, and S. Tarucha, “Interplay of Kondo and superconducting correlations in the nonequilibrium Andreev transport through a quantum dot,” *Physical Review Letters* **104**, 076805 (2010).
 - ⁷ J.-D. Pillet, C. H. L. Quay, P. Morin, C. Bena, A. Levy Yeyati, and P. Joyez, “Andreev bound states in supercurrent-carrying carbon nanotubes revealed,” *Nat. Physics* **6**, 965 (2010).
 - ⁸ K. J. Franke, G. Schulze, and J. I. Pascual, “Competition of superconductivity phenomena and Kondo screening at the nanoscale,” *Science* **332**, 940 (2011).
 - ⁹ A. Martín-Rodero and A. Levy Yeyati, “Josephson and Andreev transport through quantum dots,” *Advances in Physics* **60**, 899–958 (2011).
 - ¹⁰ A. Kumar, M. Gaim, D. Steininger, A. Levy Yeyati, A. Martín-Rodero, A. K. Hüttel, and C. Strunk, “Temperature dependence of Andreev spectra in a superconducting carbon nanotube quantum dot,” *Physical Review B* **89**, 075428 (2014).
 - ¹¹ Michael Ruby, Falko Pientka, Yang Peng, Felix von Oppen, Benjamin W. Heinrich, and Katharina J. Franke, “Tunneling Processes into Localized Subgap States in Superconductors,” *Physical Review Letters* **115**, 087001–5 (2015).
 - ¹² H. R. Krishna-murthy, J. W. Wilkins, and K. G. Wilson, “Renormalization-group approach to the Anderson model of dilute magnetic alloys. I. Static properties for the symmetric case,” *Phys. Rev. B* **21**, 1003 (1980).
 - ¹³ K. G. Wilson, “The renormalization group: Critical phenomena and the Kondo problem,” *Rev. Mod. Phys.* **47**, 773 (1975).
 - ¹⁴ Osamu Sakai, Yukihiro Shimizu, Hiroyuki Shiba, and Koji Satori, “Numerical renormalization group study of magnetic impurities in superconductors. II. Dynamical excitations spectra and spatial variation of the order parameter,” *J. Phys. Soc. Japan* **62**, 3181 (1993).
 - ¹⁵ Tomoki Yoshioka and Yoji Ohashi, “Numerical renormalization group studies on single impurity Anderson model in superconductivity: a unified treatment of magnetic, nonmagnetic impurities, and resonance scattering,” *J. Phys. Soc. Japan* **69**, 1812 (2000).
 - ¹⁶ Akira Oguri, Yoshihide Tanaka, and A. C. Hewson, “Quantum phase transition in a minimal model for the Kondo effect in a Josephson junction,” *J. Phys. Soc. Japan* **73**, 2494 (2004).
 - ¹⁷ J. Bauer, A. Oguri, and A. C. Hewson, “Spectral properties of lo-

- cally correlated electrons in a Bardeen-Cooper-Schrieffer superconductor,” *J. Phys.: Condens. Matter* **19**, 486211 (2007).
- ¹⁸ C. Karrasch, A. Oguri, and V. Meden, “Josephson current through a single Anderson impurity coupled to BCS leads,” *Phys. Rev. B* **77**, 024517 (2008).
 - ¹⁹ Ralf Bulla, Theo Costi, and Thomas Pruschke, “The numerical renormalization group method for quantum impurity systems,” *Rev. Mod. Phys.* **80**, 395 (2008).
 - ²⁰ R. Žitko, Jong Soo Lim, Rosa Lopez, and Ramon Aguado, “Shiba states and zero-bias anomalies in the hybrid normal-superconductor Anderson model,” *Phys. Rev. B* **91**, 045441 (2015).
 - ²¹ David J Luitz and Fakher F Assaad, “Weak-coupling continuous-time quantum Monte Carlo study of the single impurity and periodic Anderson models with s-wave superconducting baths,” *Physical Review B* **81**, 024509 (2010).
 - ²² E. Gull, A. J. Millis, A. I. Lichtenstein, A. N. Rubtsov, M. Troyer, and P. Werner, “Continuous-time monte carlo methods for quantum impurity models,” *Rev. Mod. Phys.* **83**, 349 (2011).
 - ²³ W. C. Oliveira and L. N. Oliveira, “Generalized numerical renormalization-group method to calculate the thermodynamical properties of impurities in metals,” *Phys. Rev. B* **49**, 11986 (1994).
 - ²⁴ Rok Žitko and Thomas Pruschke, “Energy resolution and discretization artefacts in the numerical renormalization group,” *Phys. Rev. B* **79**, 085106 (2009).
 - ²⁵ F. B. Anders and A. Schiller, “Real-time dynamics in quantum impurity systems: A time-dependent numerical renormalization group approach,” *Phys. Rev. Lett.* **95**, 196801 (2005).
 - ²⁶ Robert Peters, Thomas Pruschke, and Frithjof B. Anders, “A numerical renormalization group approach to Green’s functions for quantum impurity models,” *Phys. Rev. B* **74**, 245114 (2006).
 - ²⁷ Andreas Weichselbaum and Jan von Delft, “Sum-rule conserving spectral functions from the numerical renormalization group,” *Phys. Rev. Lett.* **99**, 076402 (2007).
 - ²⁸ A possible improvement consists in formulating the NRG truncation rule so that a comparable total number of multiplets is kept in even- and odd-fermion-parity sectors, but this has not yet been tried out.
 - ²⁹ T. Hecht, A. Weichselbaum, J. von Delft, and R. Bulla, “Numerical renormalization group calculation of near-gap peaks in spectral functions of the Anderson model with superconducting leads,” *J. Phys. Condens. Mat.* **20**, 275213 (2008).